Herschel and ALMA observations of the ISM in massive high-redshift galaxy clusters

John F. Wu,[1⋆] Paula Aguirre,[2] Andrew J. Baker,[1] Mark J. Devlin,[3] Matt Hilton,[4] John P. Hughes,[1] Leopoldo Infante,[2] Robert R. Lindner,[5] and Cristóbal Sifón[6]

⋆jfwu@physics.rutgers.edu

[1]*Rutgers, The State University of New Jersey* [2]*Pontificia Universidad Católica de Chile* [3]*University of Pennsylvania* [4]*University of KwaZulu-Natal* [5]*University of Wisconsin* [6]*Princeton University*

Introduction

Impacts of cluster environment on galaxy evolution have been studied extensively in the local universe (Dressler 1980). The hot intracluster medium (ICM) is responsible for stripping or evaporating cold gas disks (Chung et al. 2009), while tidal effects or galaxy-galaxy interactions deplete gas reservoirs that could otherwise cool and refuel star formation in the galaxy interstellar medium (ISM; Boselli & Gavazzi 2006). Most $z \sim 0$ virialized clusters reflect these quenching processes and are full of "red and dead" elliptical galaxies.

Observations of clusters at higher redshifts reveal that their populations are more likely to include blue, star-forming galaxies (Butcher & Oemler 1978). This increase in star formation rate (SFR) with redshift continues to $z \geq 1.4$ (Tran et al. 2010; Hilton et al. 2010; Hayashi et al. 2010), at which point galaxy SFRs in the dense cores of clusters *exceed* field galaxy SFRs (Brodwin et al. 2013). Abundant cool gas in high-z clusters, carried by in-falling galaxies and filaments, induces star formation activity; in a similar vein, clusters are more likely to undergo mergers at high redshifts, triggering gravitational instabilities that promote gas accretion in nuclear regions of galaxies.

Detailed observations of both the star formation *and* gas/dust content in cluster galaxies are necessary for understanding their growth during the transition phase at intermediate ($0.3 \leq z \leq 1.4$) redshifts. By targeting the most massive clusters, we can study how gas and star formation properties are impacted by the most extreme cluster environments (i.e., how galaxies might evolve in the cores versus near the outskirts of clusters). We can also investigate how cluster dynamical state (e.g., whether a cluster is merging or virialized) impacts the ISM in its member galaxies.

Sample

Our analysis focuses on four massive galaxy clusters, selected via their Sunyaev-Zel'dovich effect (SZE) decrements by the Atacama Cosmology Telescope (ACT) southern sky survey (Menanteau et al. 2010; Marriage et al. 2011; Sifón et al. 2013, 2016). ACT-CL J0102-4915 ("J0102" for short, also known as "El Gordo;" Menanteau et al. 2012) appears to be caught in the midst of a spectacular merger, whereas the other three clusters are more dynamically relaxed (Sifón et al. 2013). We summarize their basic properties in Table 1.

Cluster	z	$N_{\rm gal}$	$M_{\rm 200c}$ ($10^{14}\ M_\odot$)	*Herschel*	ALMA
ACT-CL J0235-5121	0.28	82	8.0 ± 2.9	✓	
ACT-CL J0438-5419	0.42	65	12.9 ± 3.2	✓	
ACT-CL J0102-4915	0.87	89	11.3 ± 2.9	✓	✓
ACT-CL J0546-5345	1.07	49	5.5 ± 2.3	✓	✓

Table 1: Sample of ACT SZE-selected clusters. Spectroscopic redshifts and numbers of spectroscopically confirmed members ($N_{\rm gal}$) are from Sifón et al. (2013); dynamical mass estimates are from Sifón et al. (2016).

Observations

We obtained *Herschel*/PACS and SPIRE imaging for all four clusters, which reveals dust-obscured star formation at wavelengths near the peak of the far-infrared (FIR) spectral energy distribution (SED). Additionally, we targeted the two higher-redshift clusters, J0102 and J0546, for ALMA Band 6 (~ 230 GHz) observations to study *both* the Rayleigh-Jeans tail of the dust continuum, which traces total dust mass, and CO $(4-3)$ and [C I] ($^3P_1 - {}^3P_0$) line emission, which trace dense gas mass. We also make use of *Hubble Space Telescope*/ACS, *Spitzer*/IRAC 3.6 and 4.5 μm, and Australia Telescope Compact Array (ATCA) observations of our clusters (see also Lindner et al. 2015). In Figure 1, we show an overview of the ALMA continuum observations and the locations of confirmed cluster members.

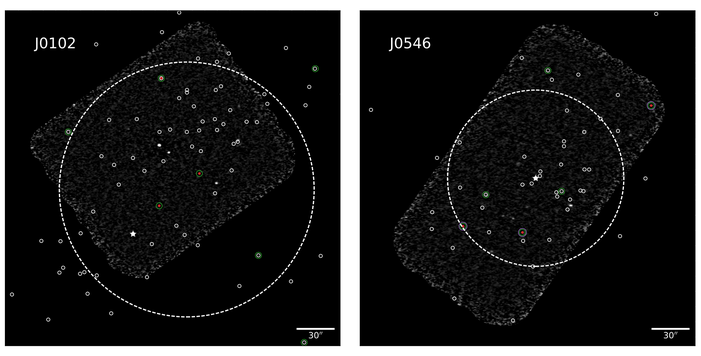

Figure 1: ALMA Band 6 continuum mosaic images shown in grayscale for our two higher-z clusters. Large dotted circles have radius $0.5 \times R_{\rm 200c}$ and are centered on the midpoint between merging components for J0102 (as determined from weak lensing measurements; Jee et al. 2014), and the brightest cluster galaxy (BCG) for J0546. Individual cluster members are identified by circular markers, from smallest to largest: ALMA CO line detections (solid red), (optically) spectroscopically confirmed galaxies (white), *Herschel*/PACS sources (green), and ALMA dust continuum sources (purple).

Results

I. Detections

We find 20 *Herschel*/PACS counterparts to confirmed cluster members across all four clusters. Six are detected in ALMA CO line emission, of which three are accompanied by ALMA dust continuum detections. (Positions of these galaxies can be seen in Figure 1.) We also measure [C I] line flux in four of the six ALMA CO line detections. The ratio of [C I] to CO $(4-3)$ in flux units is 0.54 ± 0.20. Five CO sources are newly confirmed cluster members, of which three are shown in Figure 2.

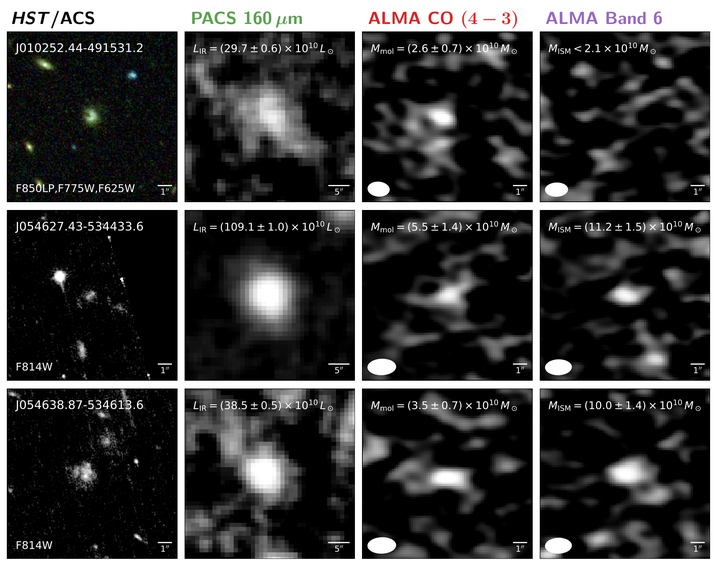

Figure 2: Postage stamp images of newly identified cluster galaxies (rows), shown in four bands (columns): *HST* imaging (rgb for J0102, grayscale for J0546), *Herschel* PACS 160 μm brightness, CO $(4-3)$ integrated line flux, and ALMA Band 6 dust continuum (all shown in grayscale). From the latter measurements we derive IR luminosity ($L_{\rm IR}$), molecular gas mass ($M_{\rm mol}$), and ISM mass ($M_{\rm ISM} \equiv M_{\rm H_2} + M_{\rm HI}$), respectively.

We find that in J0546, $M_{\rm mol}/M_{\rm ISM} = 0.55^{+0.58}_{-0.34}$, whereas in J0102, the same ratio has a nominal (and unphysical) lower limit of 1.33. It is plausible that the more violent merging state in which we are observing J0102 can explain the latter result, if higher CO excitation in its member galaxies means that we are overestimating $M_{\rm mol}$ when we scale from our observed mid-J transition.

II. Redshift evolution of infrared-bright galaxies

In order to study a luminosity-limited sample, we can consider infrared-bright galaxies (IRBGs; $L_{\rm IR} \geq 8 \times 10^{10}\ L_\odot$) . The number and fraction of IRBGs per cluster increase with redshift, as can be seen in Figure 3. For a fairer comparison across redshift, we restrict our analysis to galaxies within $r < 0.5 \times R_{\rm 200c}$. By fitting a straight-line model to the IRBG fraction as a function of redshift, we find positive slope (99% confidence interval), indicating a significant redshift evolution in the IRBG population of our massive clusters.

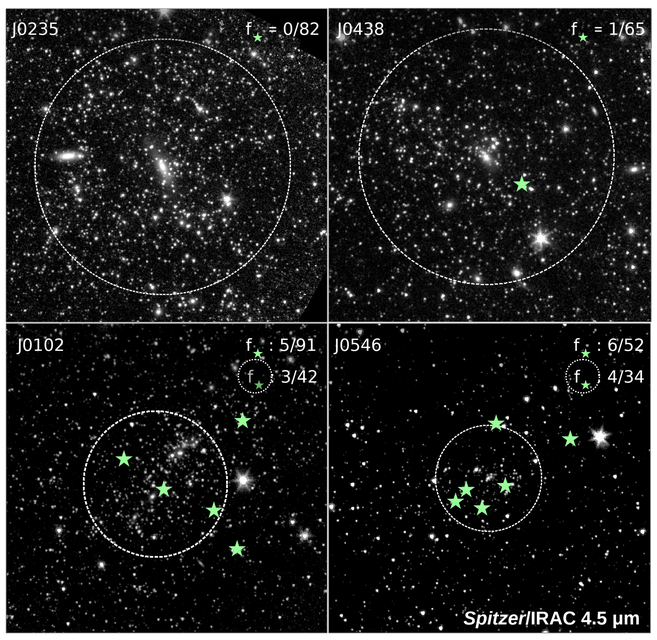

Figure 3: *Spitzer* imaging of the clusters, ordered by increasing redshift. The dotted circles have radius $0.5 \times R_{\rm 200c}$ and are centered around each cluster's BCG. Green stars (★) denote IRBGs. The fraction of IRBGs per cluster (or fraction within $r < 0.5 \times R_{\rm 200c}$ of the BCG) is shown in the upper right corner.

III. Star formation rate versus environment

We show $L_{\rm IR}$ versus projected clustercentric radius for all 20 *Herschel* counterparts in the upper panel of Figure 4. Active galactic nuclei (AGNs) are identified via a cut in the FIR-radio flux ratio ($q_{\rm IR} < 1.8$). For J0235, J0438, and J0546, we use the brightest cluster galaxy (BCG) as the cluster center; for the J0102 merger, we define the center as the midpoint between peaks in its mass distribution.

A weak trend of increasing $L_{\rm IR}$ with radius at first sight suggests a relationship between SFR and environmental density. However, diminished SFRs near cluster cores may also be a reflection of (or driven by) the SFR$-M_*$ correlation. We compute specific SFR (sSFR $\equiv$ SFR$/M_*$; stellar mass is derived from *Spitzer* photometry; Hilton et al. 2013) to separate the effects of cluster environment and galaxy mass. The lower panel of Figure 4 shows sSFR plotted against clustercentric radius, with the measured SFR$-M_*$ correlation included for comparison (Elbaz et al. 2007).

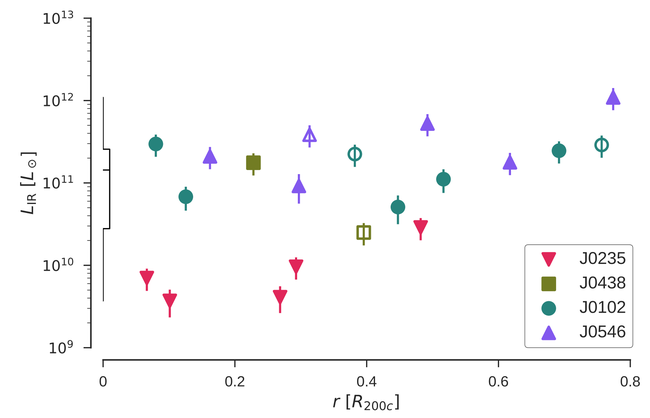

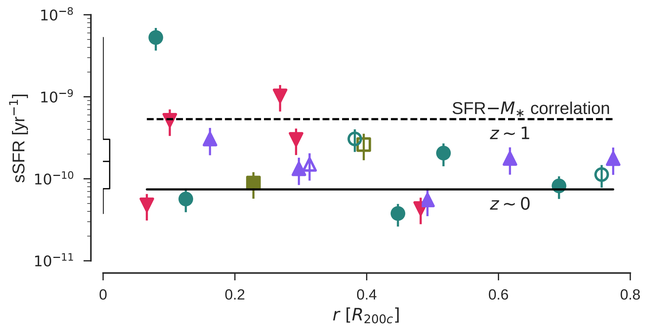

Figure 4: (*Upper*) $L_{\rm IR}$ plotted against clustercentric radius for 20 *Herschel* detections. Four confirmed AGNs are identified with open markers. On the y-axis we show an interquartile box plot. (*Lower*) Same as above, except that sSFR is plotted against clustercentric radius. We compare against the measured SFR$-M_*$ correlation for constant $\log(M_*/M_\odot) = 11.3$ at $z \sim 0$ (solid) and $z \sim 1$ (dashed).

The increase in star formation at large radii vanishes when we account for stellar mass; surprisingly, the redshift evolution of SFR disappears as well! This signifies that the cluster environment impacts the *fraction* of star-forming galaxies, but has little effect on an individual galaxy's *star formation rate*, which is instead determined by the SFR$-M_*$ correlation.

The $3\,\sigma$ outlier above the $z \sim 1$ SFR$-M_*$ correlation is J010252.44-491531.2 (also shown in the top panel of Figure 2). Its location near the midpoint between the two mass peaks of J0102 (i.e., at small radius from the merging center), where tidal effects from the cluster potential are strongest, suggests that J0102's dynamical state is driving star formation in this galaxy.

Conclusions

1. We identify 20 *Herschel*/PACS counterparts to galaxies in our sample of massive clusters, of which six are detected in CO $(4-3)$ line emission, four in [C I] emission, and three in dust continuum emission. We measure a [C I]/CO flux ratio of 0.54 ± 0.20 in flux units.
2. We find strong evidence for redshift evolution in the fraction of infrared-bright galaxies, with higher prevalence at earlier times.
3. We find modest radial trends in SFR, but these vanish when stellar mass is taken into account. Redshift and environment appear to affect the fraction of galaxies that are star-forming, but not (in general) their location relative to the SFR$-M_*$ relation.
4. We hypothesize that the dynamical state of J0102 (a) increases the CO line excitation relative to the dust continuum, and (b) elevates the sSFR in one galaxy located between its two merging components.

Acknowledgments

JFW and AJB thank Amanda Kepley for valuable support and guidance during the ALMA data reduction process. This work has been supported by (i) an award issued by JPL/Caltech in association with *Herschel*, which is a European Space Agency Cornerstone Mission with significant participation by NASA, (ii) the National Science Foundation through grant AST-0955810 and award GSSP SOSPA2-018 from the National Radio Astronomy Observatory, which is operated under cooperative agreement by Associated Universities, Inc, and (iii) a travel grant provided by the American Astronomical Society.

References

Boselli & Gavazzi (2006, PASP, 118, 517) • Brodwin et al. (2013, ApJ, 779, 138) • Butcher & Oemler (1978, ApJ, 219, 18) • Chung et al. (2009, AJ, 138, 1741) • Dressler (1980, ApJ, 236, 351) • Elbaz et al. (2007, A&A, 468, 33) • Hayashi et al. (2010, MNRAS, 402, 1980) • Hilton et al. (2010, ApJ, 718, 133) • Hilton et al. (2013, MNRAS, 435, 3469) • Jee et al. (2014, ApJ, 785, 20) • Lindner et al. (2015, ApJ, 803, 79) • Marriage et al. (2011, ApJ, 737, 61) • Menanteau et al. (2010, ApJ, 723, 1523) • Menanteau et al. (2012, ApJ, 748, 7) • Sifón et al. (2013, ApJ, 772, 25) • Sifón et al. (2016, MNRAS, 461, 248) • Tran et al. (2010, ApJL, 719, L126)